

An experimental study of the effects of pitch-pivot-point location on the propulsion performance of a pitching airfoil



Wei Tian ^{a,b}, Andrew Bodling ^b, Hong Liu ^a, James C. Wu ^a, Guowei He ^c, Hui Hu ^{b,*}

^a Center for Aerodynamics, School of Aeronautics and Astronautics, Shanghai Jiao Tong University, Shanghai 200240, China

^b Department of Aerospace Engineering, Iowa State University, Ames, IA 50010, USA

^c The State Key Laboratory of Nonlinear Mechanics, Institute of Mechanics, Chinese Academy of Sciences, Beijing 100190, China

ARTICLE INFO

Article history:

Received 6 June 2015

Accepted 23 October 2015

Keywords:

Micro-Air-Vehicles (MAVs)

Unsteady Aerodynamics

Pitching Airfoil

Pitch-pivot-point Location

PIV

ABSTRACT

An experimental investigation was conducted to characterize the evolution of the unsteady vortex structures in the wake of a pitching airfoil with the pitch-pivot-point moving from $0.16C$ to $0.52C$ (C is the chord length of the airfoil). The experimental study was conducted in a low-speed wind tunnel with a symmetric NACA0012 airfoil model in pitching motion under different pitching kinematics (i.e., reduced frequency $k=3.8\text{--}13.2$). A high-resolution particle image velocimetry (PIV) system was used to conduct detailed flow field measurements to quantify the characteristics of the wake flow and the resultant propulsion performance of the pitching airfoil. Besides conducting “free-run” PIV measurements to determine the ensemble-averaged velocity distributions in the wake flow, “phase-locked” PIV measurements were also performed to elucidate further details about the behavior of the unsteady vortex structures. Both the vorticity-moment theorem and the integral momentum theorem were used to evaluate the effects of the pitch-pivot-point location on the propulsion performance of the pitching airfoil. It was found that the pitch-pivot-point would affect the evolution of the unsteady wake vortices and resultant propulsion performance of the pitching airfoil greatly. Moving the pitch-pivot-point of the pitching airfoil can be considered as adding a plunging motion to the original pitching motion. With the pitch-pivot-point moving forward (or backward), the added plunging motion would make the airfoil trailing edge moving in the same (or opposite) direction as of the original pitching motion, which resulted in the generated wake vortices and resultant thrust enhanced (or weakened) by the added plunging motion.

© 2015 Elsevier Ltd. All rights reserved.

1. Introduction

Unsteady aerodynamics of flapping flight has attracted great attentions in aerospace engineering community over the past decades. This is driven not only by the inquisitiveness on the effective propulsion of natural flyers/swimmers, but also by the increasing interests in the development of flapping-wing-based Micro-Air-Vehicles (MAVs) for various emerging applications. Nowadays, MAVs are expected to open up revolutions for our sensing and information gathering capabilities, especially for hazardous environmental monitoring and homeland security.

* Corresponding author.

E-mail address: huhui@iastate.edu (H. Hu).

Airfoils/wings in pitching/plunge motions have been studied extensively in recent years to elucidate the fundamental underlying physics of flapping propulsion. There are a large amount of review articles to summarize the research progress of flapping-wing aerodynamics on various aspects (Ho et al., 2003; Platzer et al., 2012; Shyy et al., 2008; Wang, 2005). Knoller (1909) and Betz (1912) were among the first to propose an inviscid theory to explain that a flapping airfoil/wing can generate thrust. By analyzing a pitching flat-plate in a potential flow, Garrick (1936) found that the plate in pure pitching motion starts to generate thrust only after a relatively high pitching frequency is exceeded. Koochesfahani (1989) provided detailed flow visualization and quantitative measurements in the wake behind a pitching airfoil and reported the transition process from a drag-producing wake pattern to a thrust-producing wake pattern. Freymuth (1988), Jones et al. (1996) and Lai and Platzer (1999) measured the flow fields downstream of airfoils in pure plunging motion by using dye flow visualization and single-component laser Doppler velocimetry (LDV) technique for a range of the freestream speeds, plunging frequencies, and amplitudes of the plunging motion. They found that the vortex pattern generated by the plunging airfoil would change from drag-producing wake to thrust-producing jet flow as soon as the ratio of maximum plunge velocity to freestream speed, i.e., the non-dimensional plunge velocity, exceeds approximately 0.4. Numerous studies have been conducted since then to investigate the effects of various kinematic parameters of flapping motions on the thrust generation and propulsive efficiency of flapping airfoils/wings to uncover the underlying physics of flapping propulsion. Bohl and Koochesfahani (2009) studied the flow over a sinusoidally pitching NACA0012 airfoil of various reduced frequencies with a small pitching amplitude of 2°. Schnipper et al. (2009), Baik and Bernal (2012) experimentally investigated the effects of flapping frequency and amplitude on the evolution of the vortex structures around pitching and plunging airfoils. More recently, Yu et al. (2012a, 2012b) conducted a numerical study to investigate the effects of airfoil thickness on the thrust generation of the airfoils in pure plunging motion and to assess the contributions of pressure and viscous forces in the flapping propulsion. They found that even though the airfoils were set to undertake the same plunging motion, the thickness of the airfoils would affect the evolution of the unsteady vortex structures around the plunging airfoils significantly. After that, Yu et al. (2013) investigated the effects of airfoil thickness on flapping propulsion under different types of flapping motions, and reported that thin airfoils show superior propulsion performance in the tested range of the Reynolds numbers.

Although many important findings have been derived through the previous studies, much work is still needed in order to improve our understanding about flapping propulsion for the development of flapping-wing-based MAVs. For example, most of the previous studies on flapping airfoils were conducted with the pivot-point fixed at the quarter-chord of the airfoils. It should be noted that, the concept of quarter-chord point is actually introduced for steady aerodynamics of fixed airfoils/wings (i.e., the aerodynamic center of an airfoil is located at approximately 25% chord of the airfoil). The quarter-chord point rule derived based on steady-state aerodynamics should not be a restriction in studying unsteady aerodynamics of flapping flight. With dye injection and particle image velocimetry (PIV), OI (2007) and OI et al. (2009) experimentally investigated the effects of pivot-point location on the size and formation history of leading edge vortices (LEVs), and their subsequent behaviors in convecting over a flapping airfoil. Webb et al. (2008) conducted a numerical study to investigate how the pivot-point location may affect the aerodynamic response of a SD7003 airfoil, and the numerical simulation results are validated by the experimental data reported in OI (2007). In addition, Lian (2009) also conducted a numerical study to examine the effects of the pitch-pivot-point location on the behavior of unsteady LEVs over a flat plate. It is worth noting that, the previous studies mainly focused on the effects of pitch-pivot-point location on the evolution of LEVs that is related to the lift generation of flapping airfoils, the effects of pitch-pivot-point on the wake vortex structures and propulsion performance of flapping flight has not been explored, although this can be crucial for the optimal design of flapping-wing-based MAVs to improve their agility and maneuverability.

In the present study, we report a comprehensive experimental study to investigate the effects of the pitch-pivot-point location on the wake vortex structures and the propulsion performance of a pitching airfoil. The experiments were performed in a closed-circuit low-speed wind tunnel with a symmetric NACA0012 airfoil model undertaking a sinusoidal pitching motion at a low Reynolds number level of $Re=3\,400$. The pitch-pivot-point location was changed from $0.16C$ to $0.52C$ (C is the chord length of the airfoil) with the reduced frequency of the pitching motion ranged from $k=3.8$ to 13.2 . A high-resolution digital Particle Image Velocimetry (PIV) system was used to make detailed flow field measurements to quantify the evolution of the unsteady vortex structures in the wake behind the pitching airfoil. The characteristics of the unsteady vortex structures in the wake flow behind the pitching airfoil were analyzed in terms of the arrangement of the wake vortex pattern, peak vorticity and circulation strength. In addition to estimating the thrust coefficients of the pitching airfoil based on the ensemble-averaged flow velocity fields with an integral momentum theorem, a vorticity-moment theorem was also used to coordinate the measured vorticity fields in the wake to the thrust generation of the pitching airfoil in order to elucidate underlying physics to explore/optimize design paradigms for the development of flapping-wing-based MAVs.

2. Experimental setup

The experimental study was conducted in a closed-circuit low-speed wind tunnel located in the Aerospace Engineering Department of Iowa State University. The tunnel has a 2500 mm long \times 300 mm wide \times 300 mm high test section, and all the walls of the test section are optically transparent. The wind tunnel has a 40:1 contraction section upstream of the test

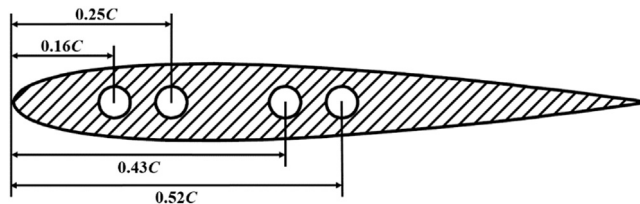


Fig. 1. Schematic of the test airfoil model.

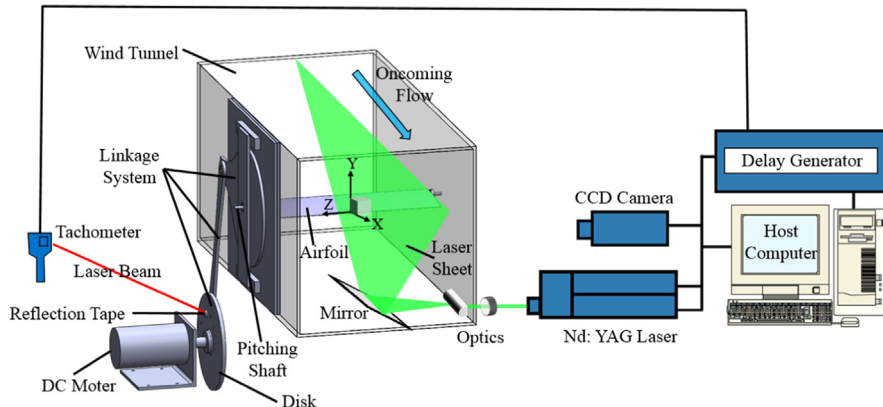


Fig. 2. Schematic of the experimental setup.

section. Honeycombs, screen structures and cooling system are installed ahead of the contraction section to provide low turbulence, uniform airflow into the test section. The turbulence level of the incoming flow was found to be within 1.0% measured by using a hotwire anemometry probe.

Fig. 1 shows the schematic of the NACA0012 airfoil model used in the present study. The airfoil model has a chord length of 100 mm (i.e., $C=100$ mm) and a span-wise length of 300 mm. The span-wise length of the airfoil model is equal to the width of the wind tunnel test section. As shown in Fig. 1, four pitch-pivot-point locations with the distance of 0.16C, 0.25C, 0.43C and 0.52C from the airfoil leading edge were used in the present study to investigate the effects of the pitch-pivot-point location on the evolution of the wake vortices and propulsion performance of the pitching airfoil. During the experiments, the wind speed of the incoming flow was fixed at 0.5 m/s (i.e., $U_\infty=0.5$ m/s), which corresponds to a chord Reynolds number of $Re_C=3\,400$.

Fig. 2 shows the schematic of the experimental setup used in the present study. A linkage system, which is driven by a servo DC motor, is used to make the airfoil in a sinusoidal pitching motion. The equation for the pitching motion is shown as

$$\alpha(t) = \alpha_0 \cos(2\pi ft + \varphi). \quad (1)$$

At all the four tested pitch-pivot-point locations, the airfoil was set to be in pitching motion with the same pitch amplitude of $\alpha_0 = 5^\circ$ about a zero mean angle of attack. The pitching frequency f was adjusted in the range of $f=3\text{--}10$ Hz, which corresponds to a reduced frequency of $k = 2\pi f C / U_\infty$ in the range of $k=3.8\text{--}13.2$.

A digital Particle Image Velocimetry (PIV) system was used in the present study to achieve detailed flow field measurements to quantify the wake characteristics behind the pitching airfoil. During the experiments, the PIV measurement plane was set in the vertical plane normal to the pitching axis of the test airfoil at the mid-span (i.e., the X-Y plane as shown in Fig. 2, the origin of the Cartesian coordinates (x, y, z) is at the mid-span of the airfoil trailing edge with the airfoil at zero angle of attack) to reveal the evolution of the unsteady wake vortex structures shedding from the trailing edge of the tested airfoil. For the PIV measurements, the incoming airflow was seeded with $\sim 1\ \mu\text{m}$ oil droplets by using a droplet generator. Illumination was provided by a double-pulsed laser adjusted on the second harmonic and emitting two pulses of 200 mJ at the wavelength of 532 nm. The thickness of the laser sheet in the measurement region was set to about 1.0 mm. A high-resolution 12-bit ($1\,376 \times 1\,040$ pixels) digital camera (SensiCam, Cooke Corp.) was used for PIV image acquisition with the axis of the camera perpendicular to the laser sheet. The digital camera and the double-pulsed Nd:YAG lasers were connected to a workstation (host computer) via a digital delay generator (Berkeley Nucleonics, Model 575), which controlled the timing of the laser illumination and the image acquisition.

After acquiring the PIV images, instantaneous velocity vectors were obtained by frame to frame cross-correlation of the patterns of particle images, using an interrogation window of 32×32 pixels. An effective overlap of 50% of the interrogation windows was employed for PIV image processing. After the instantaneous velocity vectors (u, v) were determined, instantaneous span-wise vorticity (ω_z) could be derived. In the present study, the measurement uncertainty level for the

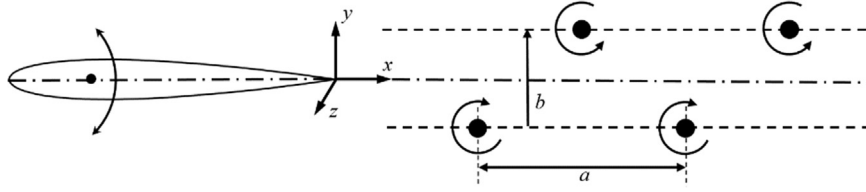


Fig. 3. Definition sketch of wake vortex pattern downstream of 2-D pitching airfoil.

velocity vectors is estimated to be within 2%, while the uncertainties for the measurements of ensemble-averaged flow quantities such as Reynolds stress and turbulent kinetic energy distributions about 5%.

In the present study, both “free-run” and “phase-locked” PIV measurements were performed. For the “free-run” PIV measurements, the acquisition rate of PIV image pairs was set to a pre-selected frequency that was not a harmonic frequency of the pitching frequency of the tested airfoil model in order to ensure physically meaningful measurements of the ensemble-averaged flow quantities. In the present study, a cinema sequence of 1000 frames of instantaneous “free-run” PIV measurements were used to calculate the ensemble-averaged flow quantities. “Phase-locked” PIV measurements were conducted to elucidate more details about the dependence of unsteady wake vortices in relation to the phase angle of the pitching airfoil model. For the “phase-locked” PIV measurements, as shown in Fig. 2, an electric reflection tape was pasted at a pre-selected location on the disk that was connected to the DC motor. With the rotation of the disk, the tachometer would generate a pulsed signal as the reflection tape passing through the laser beam emitted by the tachometer. During the experiments, the position of the laser beam was carefully adjusted to make sure that the tachometer would generate a pulsed signal at the phase angle of the test airfoil equal to $\phi=0^\circ$. The pulsed signal was then used as the input signal to a Digital Delay Generator (DDG) to trigger the digital PIV system to achieve the “phase-locked” PIV measurements. By adding different time delays between the input signal from the tachometer and the transistor-transistor logic (TTL) signal output from the DDG to trigger the digital PIV system, the “phase-locked” PIV measurements at different phase angles in a pitching motion circle could be accomplished. In the present study, 8 phase angles with steps of 45° were selected for the “phase-locked” PIV measurements. At each tested phase angle, 120 frames of instantaneous PIV measurements were used to calculate the phase-averaged flow velocity distribution.

3. Experimental results

As described in Koochesfahani (1989), the wake of a 2-D pitching airfoil can be characterized as drag-producing, neutral, or thrust-producing depending on the pitch frequency and amplitude of the pitching motion. Drag-producing wakes are found to have velocity profiles that show a momentum deficit when time averaged, typically with von Karman vortex street wake configurations with two alternating vortex rows, clockwise above and anticlockwise below. Thrust-producing wakes show a momentum surfeit, or jet, superimposed on the momentum-deficit velocity profile in the time-averaged flow, such that the thrust of the jet is greater than the inherent drag of the airfoil. The wake configuration is typically a reverse von Karman vortex street with two rows of alternating vortices with anticlockwise above and clockwise below. The definition sketch of the wake vortex pattern in the thrust-producing configuration is plotted in Fig. 3. The center of a vortex (x_c, y_c) is defined by the coordinates of its peak vorticity. The transverse spacing is defined as $b=y_{c,p}-y_{c,n}$, where $y_{c,p}$ and $y_{c,n}$ indicate the y -coordinates of the center of positive (anticlockwise) and negative (clockwise) vortices, respectively. Based on this definition, the thrust-producing configuration with the positive vortex on top results in $b > 0$, whereas $b < 0$ corresponds to the drag-producing configuration with the negative vortex on the top.

With the definition given in Fig. 3, the relationship between aerodynamic force and vorticity fields can be derived by adopting the vorticity-moment theorem developed by Wu (1981, 2005). The aerodynamic force acting on a solid body is given by

$$\vec{F} = -\rho \frac{d}{dt} \iint_{R_\infty} \vec{r} \times \vec{\omega} dR + \rho \frac{d}{dt} \iint_{R_s} \vec{v} dR, \quad (2)$$

where \vec{F} is the aerodynamic force exerted by the fluid on the solid immersed in and moving relative to the fluid, R_∞ is the region where the vorticity has a non-zero value, R_s is the region occupied by the solid, \vec{v} is the velocity field, $\vec{\omega}$ is the vorticity field, ρ is the density of the fluid, and \vec{r} is the position vector.

It can be seen that the aerodynamic force can be divided into two parts: the rate of change of the total first moment of vorticity in R_∞ and virtual mass force caused by the motion of the solid body. The virtual mass force in the thrust direction can be considered as zero due to the constant moving speed of the airfoil in this direction. Thus, the thrust induced by the vortices in the wake can be calculated as:

$$F_x = -\rho \frac{d}{dt} \iint_{R_\infty} y \cdot \omega dR = -\frac{d}{dt} (-\rho b \Gamma), \quad (3)$$

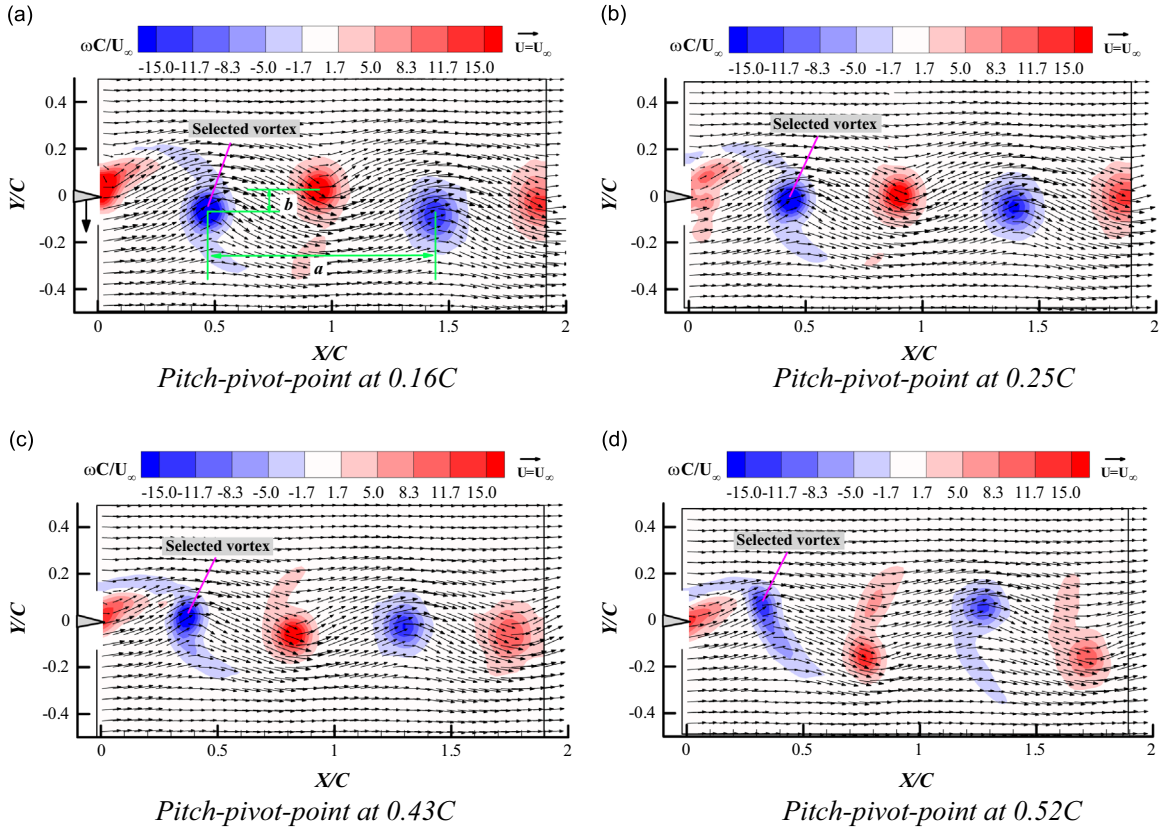


Fig. 4. Phase-locked vorticity fields with the pitch-pivot-point at different locations for the test cases of $\phi=0^\circ$ and $k=6.6$: (a) Pitch-pivot-point at $0.16C$; (b) Pitch-pivot-point at $0.25C$; (c) Pitch-pivot-point at $0.43C$; and (d) Pitch-pivot-point at $0.52C$.

$$C_T = \frac{F_x}{0.5\rho U_\infty^2 C}, \quad (4)$$

where F is the circulation of the vortex, U_∞ is the free-stream velocity, C_T is the instantaneous thrust coefficient, and C is the chord length of the test airfoil.

By integrating the instantaneous thrust in an entire pitching period, the mean thrust coefficient \bar{C}_T induced by the wake vortices can be obtained by

$$\bar{C}_T = \frac{b\bar{F}}{0.5U_\infty^2 C\tau}, \quad (5)$$

where τ is the period of the pitching airfoil, $\tau=1/f$, and \bar{F} is the averaged circulation of the wake vortex in an entire pitching period. As shown in Eq. (5), the mean thrust coefficient \bar{C}_T induced by the wake vortices is proportional to the transverse spacing (b), vortex circulation (\bar{F}), and frequency of the pitching motion (f).

Figs. 4 and 5 show the phase-averaged PIV measurement results at four selected pitch-pivot-point locations under the reduced frequency of $k=6.6$ and 12.0 , respectively. The phase angle shown in the figures is $\phi=0^\circ$, which corresponds to the airfoil at an angle of attack of $\alpha=0^\circ$, as it is pitching up (i.e., trailing edge moving down). For all the cases shown in Figs. 4 and 5, the boundary layer vorticity originating from the two sides of the pitching airfoil rolled up into an array of isolated vortices with alternating sign. Three typical wake patterns, drag-producing, neutral, and thrust-producing can be identified clearly in Figs. 4 and 5.

It can be found that the vorticity fields of different pitch-pivot-point locations reveal very different scenarios about the wake pattern. With the reduced frequency $k=6.6$, the thrust-producing wake pattern can be observed with the airfoil pitching about its $0.25C$ axis, which is consistent with the previous results obtained by Yu et al. (2012a, 2012b). With the pitch-pivot-point moving from $x/C=0.25$ to 0.16 , the wake pattern kept the thrust-producing configuration with an increase in the transverse spacing and vorticity strength. As indicated by Eq. (5), at the same reduced frequency of $k=6.6$, the generated thrust for the case with the pitch-pivot-point at $x/C=0.16$ would be higher than that of the case with the pitch-pivot-point at $x/C=0.25$. For the pitch-pivot-point at $x/C=0.43$, the wake pattern shown in Fig. 4(c) changed to the drag-producing configuration, typical of the von Karman vortex street wake with negative vortex above and positive vortex

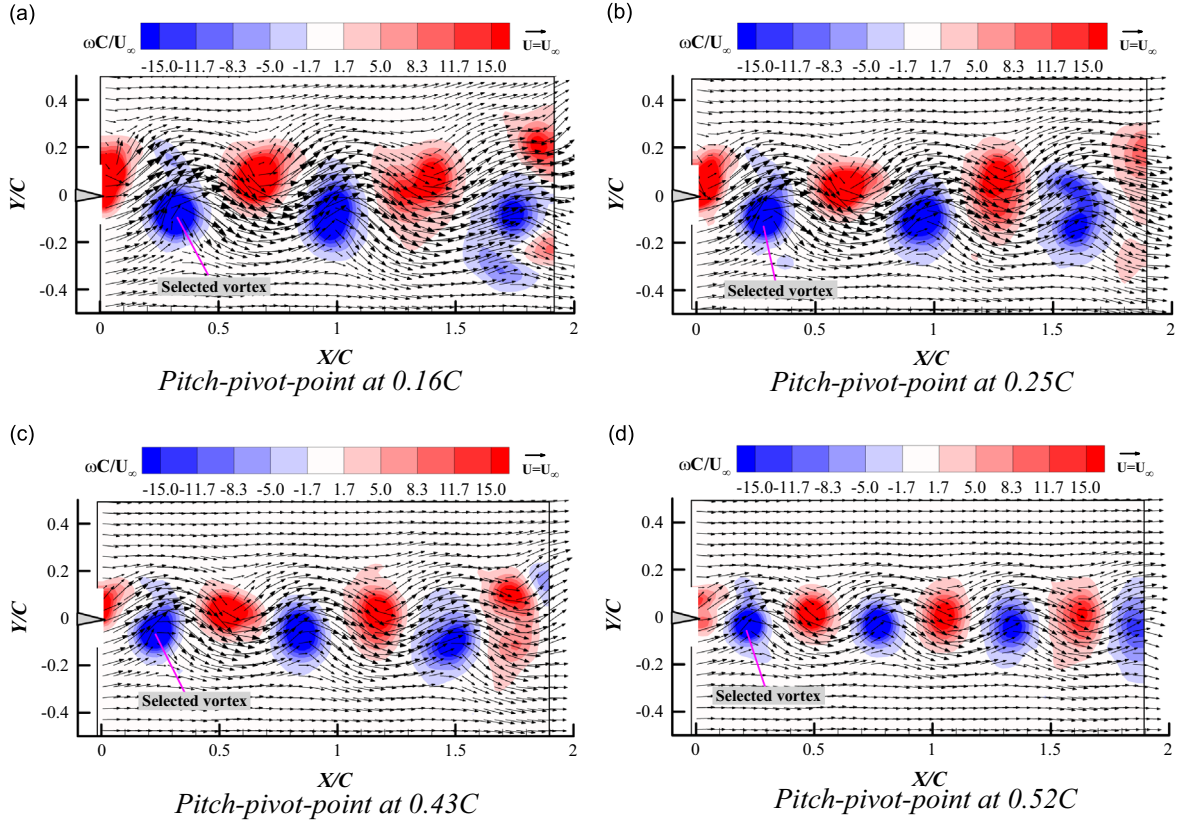


Fig. 5. Phase-locked vorticity fields with the pitch-pivot-point at different locations for the test cases of $\phi=0^\circ$ and $k=12.0$: (a) Pitch-pivot-point at $0.16C$; (b) Pitch-pivot-point at $0.25C$; (c) Pitch-pivot-point at $0.43C$; and (d) Pitch-pivot-point at $0.52C$.

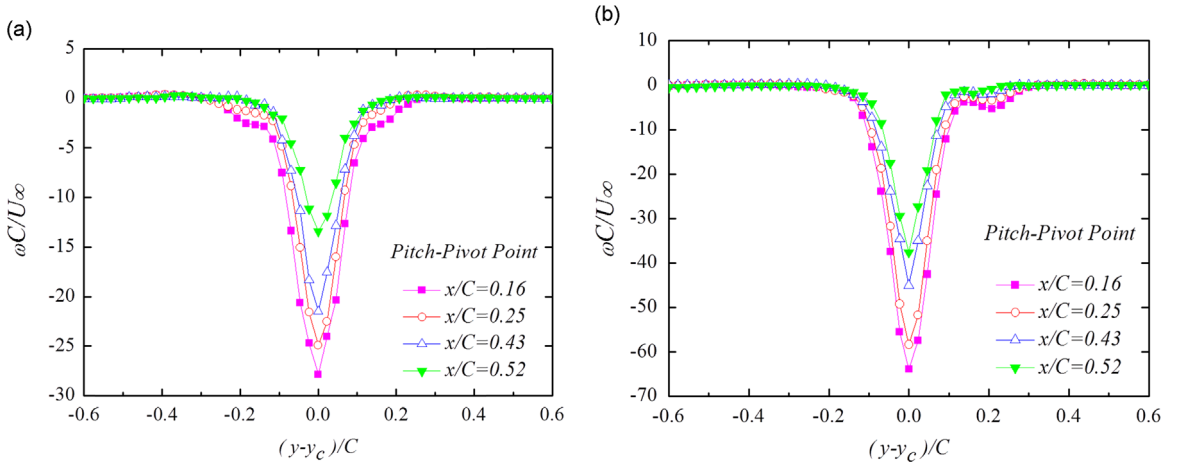


Fig. 6. Transverse profiles of the vorticity in the wake for the cases of (a) $k=6.6$ and (b) $k=12.0$.

below. As observed in Fig. 4(d), as the pitch-pivot-point moving further to the trailing edge (i.e., $x/C=0.52$), the wake pattern became the drag-producing configuration and the transverse spacing between the negative and positive vortex significantly increased.

As shown in Fig. 5, the wake pattern of all four pitch-pivot-point locations changed to the thrust-producing configuration with the reduced frequency increased to $k=12.0$. For the test case with the pitch-pivot-point at $x/C=0.16$, the strong interaction between neighboring positive and negative vortices affected the wake flow significantly. With the flow moving downstream, the shedding vortex first deformed into an irregular shape, then broke down and turned into smaller and weaker vortices. After the breakdown of the concentrated vortices, the mixing of the positive and negative vortices, as well as the wake expansion in the transverse direction, could be clearly observed as the wake flow moving further downstream.

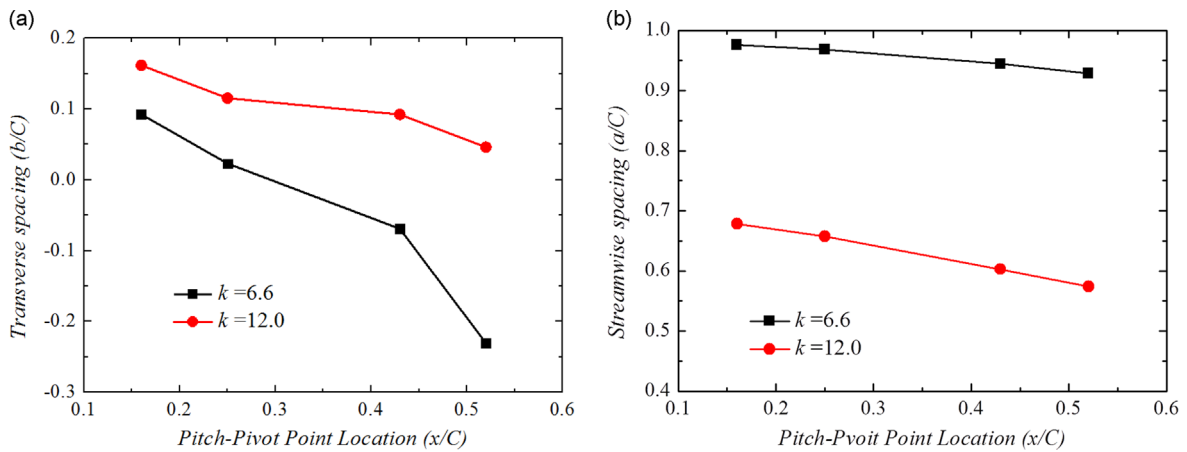


Fig. 7. Variations of (a) transverse spacing and (b) stream-wise spacing as a function of the pitch-pivot-point location for the test cases of $k = 6.6$ and 12.0.

However, with the pitch-pivot-point moving towards the trailing edge of the airfoil, the interaction between the wake vortices gradually diminished even under the same reduced frequency. As shown in Fig. 5(d), the phenomena of the deformation and breakdown of vortices in the wake have disappeared. Only a decrease in the magnitude of vorticity strength can be observed with the wake vortex moving further downstream, which is mainly caused by the viscous dissipation. A similar continuously decreasing trend of vorticity strength was also reported by Bohl and Koochesfahani (2009).

Fig. 6 shows the transverse profiles of the vorticity distribution (i.e., vorticity variation in y direction) through the center of the fully developed wake vortex shedding from the airfoil trailing edge. The selected wake vortices used to extract the vorticity profiles are marked in Figs. 4 and 5. As shown in Fig. 6, the vorticity profiles of the selected wake vortices were found to fit well with Gaussian distributions. The peak vorticity (i.e., maximum vorticity at the center of the wake vortex) was found to decrease monotonically as the pitch-pivot-point moving towards the airfoil trailing edge. The wake vortex with pitch-pivot-point at $x/C=0.16$ had the highest peak vorticity, which was found to be almost twice of that with the pitch-pivot-point at $x/C=0.52$. However, due to the strong interaction between neighboring wake vortices for the test case with higher reduced frequency of $k=12.0$, the vorticity profiles for the test cases with the pitch-pivot-point closer to the airfoil leading edge did not keep a Gaussian distribution shape as the wake vortex moving further downstream, which can be observed clearly in Fig. 5.

The spacing between the vortex structures in the wake is another important parameter to affect the evolution of the wake vortices, as well as the propulsion performance of the pitching airfoil. The transverse spacing (b) and stream-wise spacing (a) extracted from the vorticity distributions shown in Figs. 4 and 5 are plotted in Fig. 7. As shown in Fig. 4(a), the transverse spacing (b) is defined as the vertical distance between the fully developed negative and positive vortices near to the airfoil trailing edge. The stream-wise spacing (a) is defined as the horizontal distance between the neighboring negative vortices which were also near to the airfoil trailing edge. As shown in Fig. 7(a), with the same reduced frequency of $k=6.6$, the sign switch of the transverse spacing (b) clearly indicate that the wake pattern behind the pitching airfoil would change from thrust-producing to drag-producing with the pitch-pivot-point moving from $x/C=0.25$ to 0.43. With the increase of the reduced frequency, the wake flow pattern for the cases with the pitch-pivot-point at $x/C=0.43$ and 0.52 would first change from drag-producing to the neutral configuration. In the neutral configuration, the generated thrust due to the pitching motion would be balanced by the inherent drag with the positive and negative wake vortices arranged in one column ($b=0$). As the reduced frequency increases, the wake pattern behind the pitching airfoil was then found to change into the thrust-producing configuration ($b > 0$). For the test cases with the reduced frequency of $k=12.0$, the wake pattern behind the pitching airfoil was found to be in thrust-producing configuration for the test cases with the pitch-pivot-point at all four tested locations. Also, the transverse spacing, depicted in Fig. 7(a), showed a decrease trend as the pitch-pivot-point moving towards the airfoil trailing edge. In addition, as shown in Fig. 7(b), the stream-wise spacing (a) show a linear decreasing trend as the pitch-pivot-point moving towards the airfoil trailing edge. The vortex traveling velocity U_c is related to the stream-wise spacing a and the pitching frequency f through $U_c=af$. Therefore, the curves shown in Fig. 7(b) also indicate the linear relationship between the vortex traveling velocity and the pitch-pivot-point location with the reduced frequency kept same during the experiments.

As described in Eq. (5), the propulsion induced by the wake vortices for a pitching airfoil is proportional to the transverse spacing (b) and vortex circulation (\bar{T}). In the present study, the vortex circulation was computed from the area integral of the phase-averaged vorticity distributions. In order to exclude the vorticity measurement noise, only vorticity magnitudes over a cut-off limit of $\omega=5 \text{ s}^{-1}$ (i.e., $\omega C/U_\infty > 1.0$) were included in calculating the vortex circulation. The vortices selected for the circulation calculation are the fully developed vortex structures near the airfoil trailing edge (i.e., the vortices marked in Figs. 4 and 5) at the phase angle of $\phi=0^\circ$. As shown in Figs. 4 and 5, in order to minimize the contributions from the

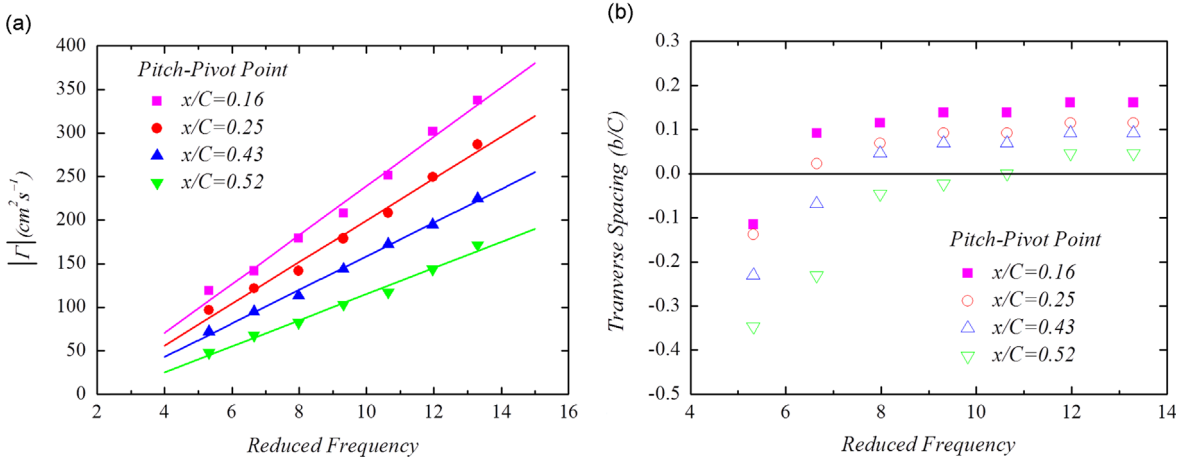


Fig. 8. Variations of (a) vortex circulation and (b) transverse spacing as a function of the reduced frequency with the pitch-pivot-point at different locations.

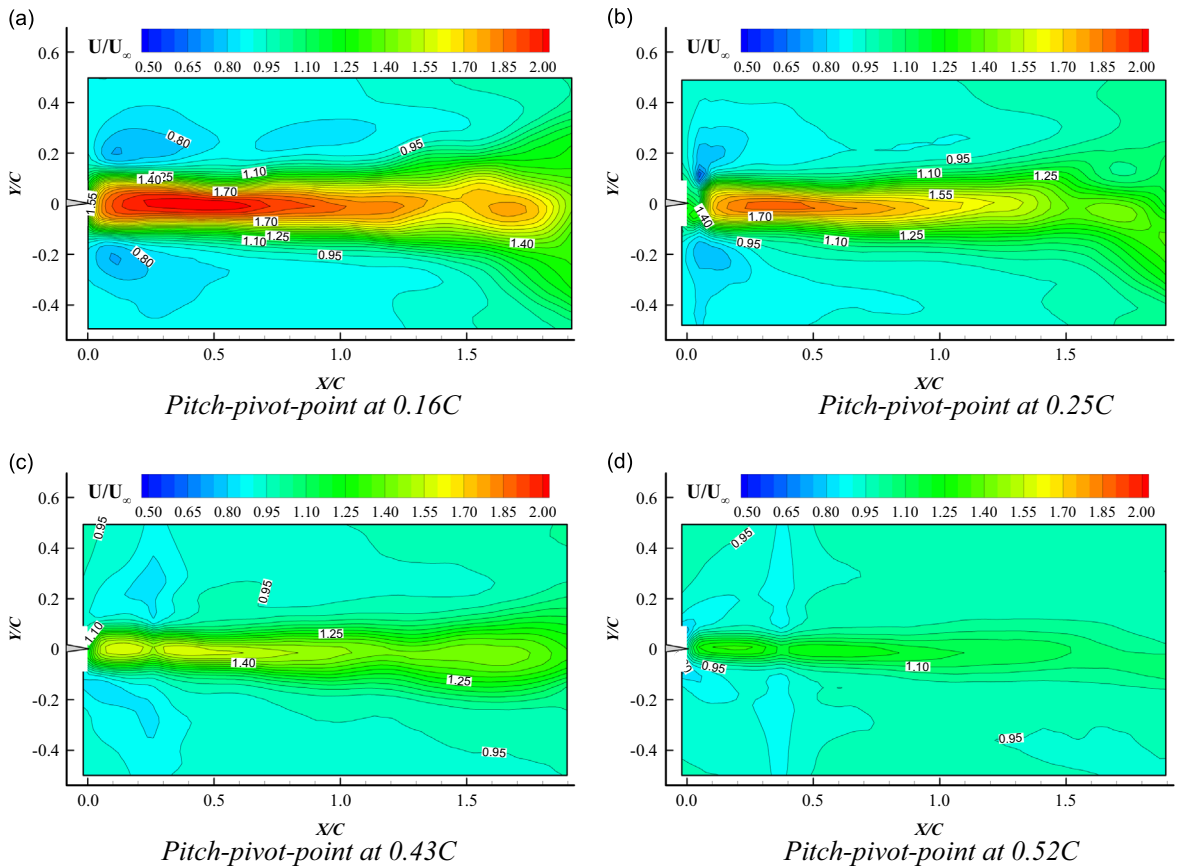


Fig. 9. Ensemble-averaged velocity fields for four pitch-pivot-point locations, $k=12.0$: (a) Pitch-pivot-point at $0.16C$; (b) Pitch-pivot-point at $0.25C$; (c) Pitch-pivot-point at $0.43C$; and (d) Pitch-pivot-point at $0.52C$.

neighboring vortices of opposite sign and the connecting braids, the integration area for the circulation calculation was limited to a radius of 1.5 cm from the vortex center.

Based on the definition given above, the variations of the vortex circulation (Γ) at the phase angle of $\phi=0^\circ$ and transverse spacing (b) as a function of the reduced frequency with the pitch-pivot-point at different locations are plotted in Fig. 8. The linear relationship between the vortex circulations and the reduced frequency of the pitching motion can be observed clearly from the measurement data given in Fig. 8(a). With the same reduced frequency, the vortex circulation was found to decrease continuously as the pitch-pivot-point moving from $x/C=0.16$ to 0.52 . In addition, the slope of the fitted lines shown

in Fig. 8(a) reveals a much higher growth rate of the vortex circulation for the test cases with the pitch-pivot-point being closer to the leading edge of the airfoil model.

For the test cases with the pitch-pivot-point fixed at the same location, the transverse spacing b was found to be initially negative, corresponding to the von Karman vortex street pattern with the negative vortices above the positive vortices. With the increasing pitching frequency of the airfoil, the transverse spacing b was found to become zero (i.e., neutral configuration with the positive and negative vortices array aligned in one column) and then switched to a positive value, which corresponds to the reverse von Karman vortex street pattern with the positive vortices above the negative vortices. As shown in Fig. 8(b), the frequency at which the wake transitioned from drag producing to thrust producing was found to be significantly affected by the location of the pitch-pivot-point. While the wake pattern for the case with the pitch-pivot-point at $x/C=0.16$ became the neutral configuration around the reduced frequency of $k=6.0$, the frequency at which the transition occurred for the case with the pitch-pivot-point at $x/C=0.52$ was found to be delayed until $k=10.6$. The measurement results given in Fig. 8(b) also reveal that, for the test cases with the pitch-pivot-point fixed at the same location, the transverse spacing would approach a constant value with the reduced frequency becoming big enough. However, with the pitch-pivot-point moving towards the trailing edge, a higher reduced frequency is needed to approach this constant value.

Fig. 9 shows the ensemble-averaged velocity fields behind the pitching airfoil with the pitch-pivot-point of the airfoil changed from $0.16C$ to $0.52C$, which were obtained based on time sequences of 1 000 frames of instantaneous PIV results for each test case. It reveals clearly that, even though the reduced frequency of the pitching motion is fixed at $k=12.0$, the characteristics of the wake flow behind the pitching airfoil would vary dramatically as the pitch-pivot-point location of the pitching airfoil changes. Fig. 10 shows the transverse profiles of the streamwise flow velocity extracted from the ensemble-averaged velocity fields at the downstream location of $x/C=1.0$, which can be used to reveal the effects of the pitch-pivot-point locations on the characteristics of the wake flow more clearly and quantitatively.

It can be seen clearly that for the test cases with a relatively low reduced frequency of $k=6.6$, the mean velocity profiles behind the pitching airfoil would change from momentum surfeits to deficits as the pitch-pivot-point was moved from $x/C=0.25$ to 0.43 , which is coincident with the observation obtained from the vorticity fields described above (i.e., changing from thrust-producing to drag-producing configuration). For the test cases with a relatively high reduced frequency of $k=12.0$, the velocity profiles behind the pitching airfoil show momentum surfeits for all the test cases with the pitch-pivot-point at four different locations. As shown in Fig. 10, the peak velocity in the wake behind the pitching airfoil was found to increase continuously as the pitch-pivot-point moving toward the airfoil leading edge. More specifically, the peak velocity for the case with the pitch-pivot-point at $x/C=0.16$ was found to be $1.86U_\infty$, which is about 60% higher than that of the case with the pitch-pivot-point at $x/C=0.52$ at the same reduced pitching frequency of $k=12.0$. In addition, the high-speed jet in the wake flow was also found to have a greater width with the pitch-pivot-point moving closer to the airfoil leading edge, which corresponds to the larger transverse spacing between neighboring positive and negative vortices as shown in Fig. 7(a).

With the ensemble-averaged flow velocity fields as those given in Fig. 9, the time-averaged thrust force generated by the pitching airfoil can be obtained by applying the integral momentum theorem to a control volume surrounding the airfoil. Following the work of Bohl and Koochesfahani (2009), the thrust coefficient of the pitching airfoil was estimated by using

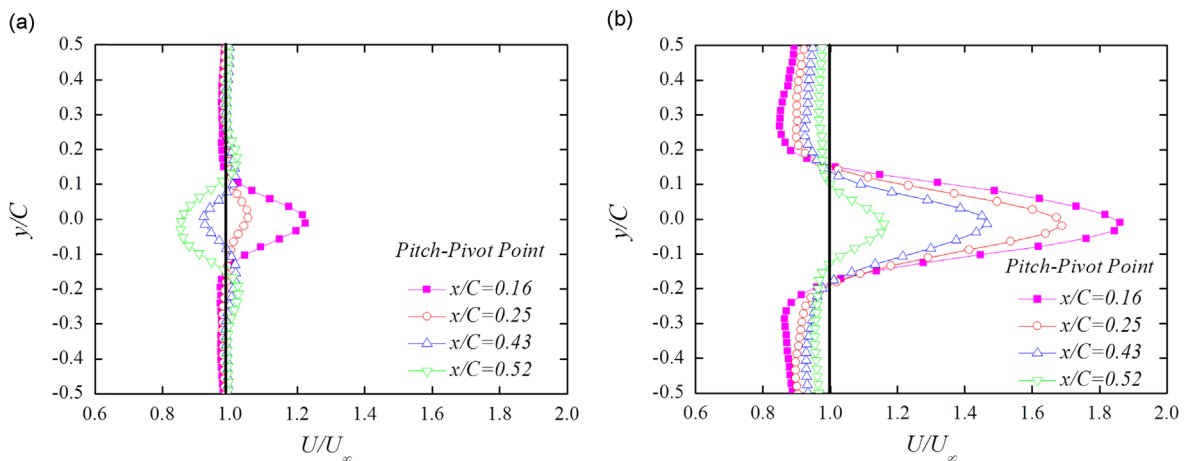


Fig. 10. Vertical profiles of the ensemble-averaged stream-wise velocity at $x/C=1.0$ for the test cases with the reduced frequency of (a) $k=6.6$ and (b) $k=12.0$.

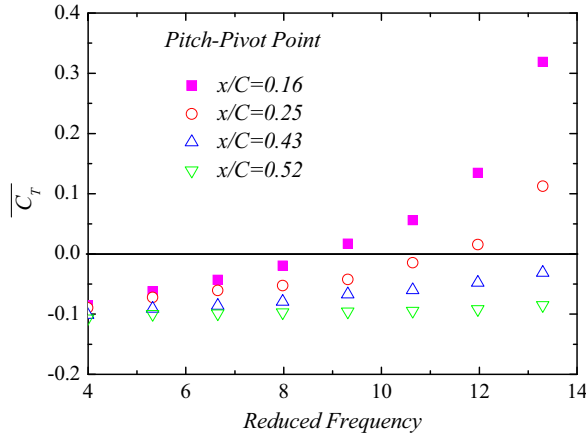


Fig. 11. Variation of mean thrust coefficient \bar{C}_T with reduced frequency under different pitch-pivot-point locations.

the following equation:

$$\bar{C}_T = \frac{2}{C} \int_{-H}^H \left\{ \underbrace{\frac{u(y)}{U_\infty} \left(\frac{u(y)}{U_\infty} - 1 \right)}_{\text{1st term}} + \underbrace{\epsilon \left(\frac{u(y)}{U_\infty} - 1 \right)}_{\text{2nd term}} + \underbrace{\frac{1}{2} \left(1 - \frac{U_o^2}{U_\infty^2} \right)}_{\text{3rd term}} + \underbrace{\left(\frac{u_{rms}}{U_\infty} \right)^2 - \left(\frac{v_{rms}}{U_\infty} \right)^2}_{\text{4th term}} \right\} dy \quad (6)$$

where $u(y)$ is the mean stream-wise velocity profile in the wake, u_{rms} and v_{rms} are the turbulent velocity fluctuations in the streamwise and transverse directions, respectively.

Traditionally, only the 1st term on the right-hand side of the Eq. (6) is considered to calculate the thrust coefficient of a stationary airfoil by applying integral momentum theorem to a control volume surrounding the airfoil. However, as described in Bohl and Koochesfahani (2009), since the wake flow behind a pitching airfoil is highly unsteady, additional terms are added on the right-hand side of Eq. (6) to take the unsteady feature of the wake flow into account in estimating the thrust force generated by the pitching airfoil. Since the wake flow behind a pitching airfoil would become much wider in comparison with that of a stationary airfoil, with the limited size of the measurement window used in the present study, the ‘free-stream’ velocity U_o in the wake behind the pitching airfoil may become different from the incoming flow velocity, U_∞ , upstream of the airfoil. The 2nd and the 3rd terms on the right-hand side of Eq. (6) are introduced to consider the effects of the velocity difference between U_o and U_∞ on the thrust force estimation, and ϵ can be calculated based on $\frac{1}{2}(U_\infty + U_o) = (1 - \epsilon)U_\infty$. As shown in Fig. 10(a), the differences between U_o and U_∞ were found to be relatively smaller for the test cases with a relatively low reduced frequency (i.e., $k=6.6$ case), and the change of the pitch-pivot-point location has no significant effects on U_o in the wake flow. However, as shown in Fig. 10(b), the differences between U_o and U_∞ become much more significant for the cases at a relatively high reduced frequency (i.e., $k=12.0$ case) with the momentum surfeits in the wake being much greater. With the pitch-pivot-point moving closer to the airfoil leading edge, the flow velocity U_o in the wake was found to become significantly smaller than the incoming flow velocity, U_∞ . Therefore, the 2nd and 3rd terms on the right-hand side of Eq. (6) become very important in the assessment of the propulsion performance of the pitching airfoil, especially for the test cases at relatively high reduced frequencies.

It should also be noted that the turbulent velocity fluctuations in the wake of a stationary airfoil at relative small angles of attack ($< 10^\circ$) are usually quite small, and their effects are usually neglected in applying the integral momentum theorem to calculate of the mean force acting on the stationary airfoil. However, as shown in the PIV measurement results given above, with the maximum pitching angle of the airfoil being only 5.0° , the wake flow behind the pitching airfoil was found to become highly unsteady with significant turbulent velocity fluctuations. As suggested by Bohl and Koochesfahani (2009), the significant turbulent velocity fluctuations in the wake behind a pitching airfoil would also affect the thrust force generation of a pitching airfoil. While the streamwise velocity fluctuation u_{rms} is beneficial for the thrust force generation, the transverse velocity fluctuation v_{rms} will be responsible for lowering the downstream pressure, resulting in a net reduction of the mean thrust force generated by the pitching airfoil. Therefore, the 4th term is added on the right-hand side of Eq. (6) with the consideration of the effects of the turbulent velocity fluctuations.

By using Eq. (6), the variations of the estimated thrust coefficient \bar{C}_T as a function of the reduced frequency of the pitching airfoil with the pitch-pivot-point at different locations are plotted in Fig. 11. It should be noted the negative thrust data shown in the plot represent that the streamwise aerodynamic forces acting on the pitching airfoil are actually drags, instead of thrusts. As expected, the streamwise force was initially drag (i.e., negative thrust) and increased monotonically as the reduced frequency increases. The measurement data given in Fig. 11 also reveals clearly that, with the same reduced frequency, the mean thrust produced by the pitching airfoil would increase continuously as the pitch-pivot-point moving

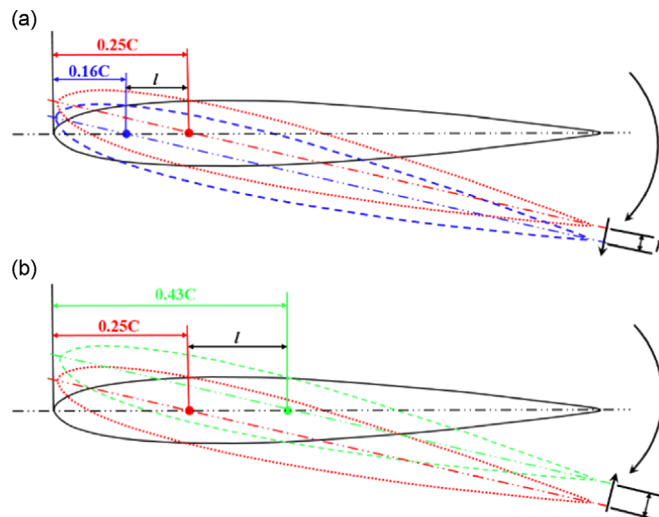


Fig. 12. The schematic of the pitching motions at different pitch-pivot-point locations.

towards the leading edge of the airfoil, which is coincident with the conclusions derived from the analysis of the vorticity distribution described above. In addition, the increase rates of the mean thrust coefficients with the increasing reduced frequency were also found to be highly affected by the location of the pitch-pivot-point. As the reduce frequency increases from $k=3.8$ to 13.2 , while the thrust coefficients for the test cases with the pitch-pivot-point at $x/C=0.16$ were found to have the most rapid increase rate, only a marginal decrease of the drag can be achieved for the test cases with the pitch-pivot-point located at $x/C=0.52$.

It should also be noted that the critical reduced frequency for the crossover from the drag-producing to the thrust-producing configuration based on the analysis of the vorticity distributions (i.e., neutral configuration with positive and negative vortices array in one column with transverse spacing $b=0$) was found to be much smaller than the critical frequency revealed from the calculated thrust force by using Eq. (6). For example, while the critical reduced frequency shown in Fig. 8(b) is around $k=6.3$ for the test cases with the pitch-pivot-point located at $x/C=0.25$, the critical reduced frequency for the crossover shown in Fig. 11 was found to be around $k=11.0$. Moreover, for the test cases with the pitch-pivot-point at $x/C=0.43$ and 0.52 , the upper limit of the tested reduced frequency (i.e., $k=13.2$) is not even high enough for the streamwise force to change from drag to thrust. As explained by Bohl and Koochesfahani (2009), this phenomena is mainly caused by the large transverse velocity fluctuation v_{rms} , which is responsible for the pressure reduction downstream of the pitching airfoil, resulting in a net reduction of the stream-wise force acting on the pitching airfoil.

4. Discussions

As revealed from the measurement results described above, the location of the pitch-pivot-point was found to affect evolution of the wake vortices and the propulsion performance of a pitching airfoil significantly. Fig. 12 shows schematically the comparison of the pitching motions with the pitch-pivot-point at different locations, which can be used to explain the experimental observations described above. In the analysis, the test case with the pitch-pivot-point at $x/C=0.25$ is used as the baseline case in comparison with the cases with the pitch-pivot-point at other locations.

As described in Section 2, the effective angle of attack of the pitching airfoil at a fixed time (i.e., $t=t_0$) can be expressed as $\alpha(t_0)=\alpha_0 \cos(2\pi f t_0 + \varphi)$, which has no relationship with the pitch-pivot-point location. As shown in Fig. 12, the pitching motion with the pitch-pivot-point at any other location can actually be considered as a pitching motion with the pitch-pivot-point at $x/C=0.25$ superposition onto a plunging motion. The angle of attack of the plunging motion is $\alpha(t_0)$, and the plunge amplitude h can be expressed as

$$h(t_0) = l \sin \alpha(t_0) \quad (7)$$

where l is the distance between the two compared pitch-pivot-points.

As shown in Fig. 12(a), with the pitch-pivot-point moving forward from $x/C=0.25$ to 0.16 , the added plunging motion would make the airfoil trailing edge to move in the same direction as driven by the original pitching motion with the pitch-pivot-point at $x/C=0.25$. However, with the pitch-pivot-point moving from $x/C=0.25$ towards the trailing edge, as shown in Fig. 12(b), the added plunging motion would cause the airfoil trailing edge moving in the opposite direction from that of the original pitching motion. Obviously, the two scenarios can be considered as the cases with opposite phase lags between the pitching and plunging motions. It should be noted that, as reported in Jones and Platzer (1997) and Schouweiler et al. (2005), a better propulsive performance can be achieved when a suitable phase lag was adopted for an airfoil in combined pitching and plunging motion.

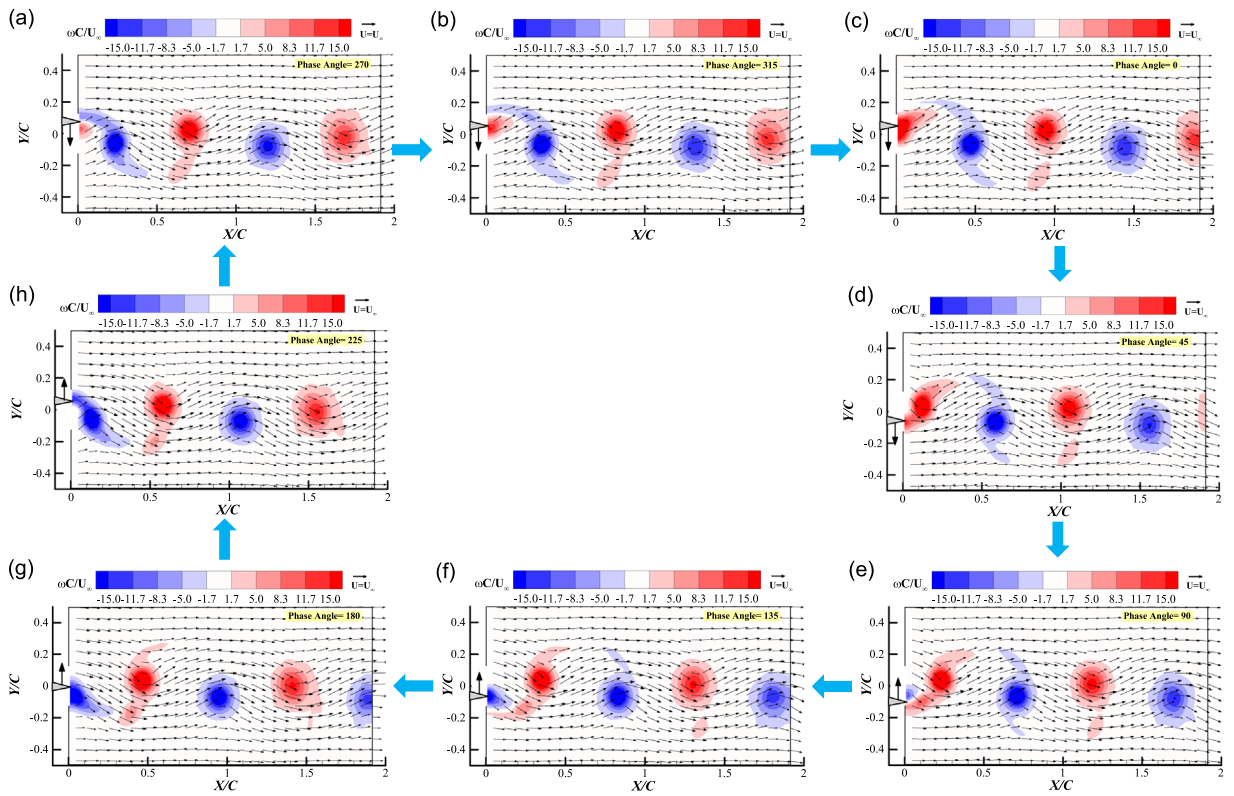


Fig. 13. Phase-locked PIV measurement results during a pitching cycle ($k=6.6$, pitch-pivot-point: $x/C=0.16$): (a) $\phi=270^\circ$, trailing edge at the upmost position and start moving down; (b) $\phi=315^\circ$, trailing edge moving down; (c) $\phi=0^\circ$, trailing edge moving down; (d) $\phi=45^\circ$, trailing edge moving down; (e) $\phi=90^\circ$, trailing edge at the down most position and start moving up; (f) $\phi=135^\circ$, trailing edge moving up; (g) $\phi=180^\circ$, trailing edge moving up; (h) $\phi=225^\circ$, trailing edge moving up.

It is well known that the generation of wake vortices near the airfoil trailing edge is due to the pressure differences between the upper and lower sides of the pitching airfoil. Fig. 13 shows typical phase-locked PIV measurements results to reveal the evolution of the unsteady vortex structures in the wake during one pitching cycle. It is revealed clearly that, while the airfoil leading edge is pitching up (i.e., trailing edge moving down), due to the higher pressure on the lower side of the airfoil than that of the upper side, the boundary layer near the airfoil trailing edge would roll up from the lower side to the upper side. With the trailing edge moved to the lowest position, as shown in Fig. 13(e), a positive vortex (i.e., anti-clockwise) was found to be formed and shed from the airfoil trailing edge in the wake. With the trailing edge moving up from the lowest position, while a positive vortex (i.e., anti-clockwise) would move further downstream in the wake, a new negative vortex (i.e. clockwise) was found to form since the pressure on the upper side of the airfoil would be higher than that on the lower side. The negative vortex (i.e., clockwise) would subsequently shed from the pitching airfoil as the airfoil trailing edge moved to the highest position, as shown clearly in Fig. 13(e)–(h).

As described above, with the pitch-pivot-point moving forward, the added plunging motion would be in phase with the original pitching motion. The pressure difference between the upper and lower sides of the airfoil would be enhanced by the added plunging motion. A positive (i.e., anti-clockwise) vortex with much greater strength would be formed on the lower side and shed subsequently as the trailing edge reaches its lowest position. Similarly, as the airfoil is pitching down (i.e., trailing edge moving up), the added upstroke of the plunging motion would enhance the negative (i.e., clockwise) vortex shedding from the upper side of the pitching airfoil. However, with the pitch-pivot-point moving towards the trailing edge, the added upstroke of the plunging motion would be out of phase with the original pitching motion. The added upstroke of the plunging motion would weaken the pressure difference between the upper and lower sides of the airfoil, which apparently decrease the strength of the positive vortex induced by the original pitching motion with the pitch-pivot-point at $x/C=0.25$.

5. Conclusions

An experimental investigation was conducted to investigate the effects of the pitch-pivot-point on the evolution of the wake vortices and the results propulsion performance of a pitching airfoil. The experimental study was conducted in a low-speed wind tunnel at a low Reynolds number level of $Re=3\,400$. A symmetric NACA0012 airfoil model was set to be in pitching motions with the pitch-pivot-point changing from $0.16C$ to $0.52C$ (C is the chord length of airfoil) and reduced

frequency, k , in the range of 3.8–13.2. A high-resolution particle image velocimetry (PIV) system was used to conduct detailed flow field measurements to quantify the characteristics of the wake flow and the resultant propulsion performance of the pitching airfoil. It was found that, even though the airfoil was set to pitch at the same reduced frequency, the evolution of the wake vortex structures and the resultant thrust force generated by the pitching airfoil varied significantly due to the change of the pitch-pivot-point location.

Based on vorticity-moment theorem, the thrust induced by the wake vortices was found to be proportional to the circulation of vortex (Γ), transverse spacing (b) and the frequency of the pitching motion (f). Under the same reduced frequency, both the circulation and transverse spacing of the wake vortices were found to increase monotonously as the pitch-pivot-point is moved forward to approach the airfoil leading edge. By applying the integral momentum theorem to a control volume surrounding the airfoil, the thrust coefficients of the pitching airfoil with the pitch-pivot-point at different locations were calculated based on the ensemble-averaged PIV measurement results. The estimated thrust generated by the pitching airfoil showed a continuously increased trend as the pitch-pivot-point moving towards the airfoil leading edge, which is coincident with the conclusions derived from the analysis of the vorticity-moment theorem.

In summary, the location of the pitch-pivot-point was found to affect the characteristics of wake flow and resultant propulsion performance of a pitching airfoil significantly. Moving the pitch-pivot-point of a pitching airfoil forward (or backward) is equivalent to add a plunging motion to the original pitching motion, which would make an advantageous (or disadvantageous) influence on the generation and shedding of the wake vortices and the resultant thrust force generated by the pitching airfoil.

Acknowledgment

The support from National Science Foundation, United States (NSF) with Grant No. of IRES-1064235 and Opening fund of State Key Laboratory of Nonlinear Mechanics, Chinese Academy of Sciences, China are gratefully acknowledged.

References

- Baik, Y., Bernal, L., 2012. Experimental study of pitching and plunging airfoils at low Reynolds numbers. *Experiments in Fluids* 53, 1979–1992.
- Betz, A., 1912. Ein Beitrag zur Erklarung des Segelfluges. *Zeitschrift fur Flugtechnik und Motorluftschiffahrt* 3, 269–272.
- Bohl, D., Koochesfahani, M., 2009. MTV measurements of the vortical field in the wake of an airfoil oscillating at high reduced frequency. *Journal of Fluid Mechanics* 620, 63–88.
- Freyymuth, P., 1988. Propulsive vortical signatures of plunging and pitching airfoils. *AIAA Journal* 26 (7), 881–883.
- Garrick, I.E., 1936. Propulsion of a Flapping and Oscillating Airfoil, NASA Report 567.
- Ho, S., Nassef, H., Pornsinsirirak, N., 2003. Unsteady aerodynamics and flow control for flapping wing flyers. *Prog. Aerosp. Sci.* 39, 635–681.
- Jones, K.D., Dohring, C.M., Platzer, M.F., 1996. Wake structures behind plunging airfoils: a comparison of numerical and experimental results. In: 34th Aerospace Sciences Meeting and Exhibit, Reno, NV, AIAA-1996-0078.
- Jones, K.D., Platzer, M.F., 1997. Numerical computation of flapping-wing propulsion and power extraction. In: Proceedings of the 35th AIAA Aerospace Sciences Meeting & Exhibit Reno, Nevada, January 6–9. AIAA-1997-0826.
- Knoller, R., 1909. Die Gesetze des Luftwiderstandes. *Flug- und Motortechnik (Wien)* 3, 1–7.
- Koochesfahani, M., 1989. Vortical patterns in the wake of an oscillating airfoil. *AIAA Journal* 27, 63–88.
- Lai, J.S., Platzer, M., 1999. Jet characteristics of a plunging airfoil. *AIAA Journal* 37, 1529–1537.
- Lian, Y.S., 2009. Parametric study of a pitching flat plate at low Reynolds Numbers. In: 39th AIAA Fluid Dynamics Conference, San Antonio, TX, AIAA-2009-3688.
- Ol, M., 2007. Vortical structures in high frequency pitch and lunge at low Reynolds number. In: 37th AIAA Fluid Dynamics Conference and Exhibit, Miami, FL. AIAA-2007-4233.
- Ol, M.V., Eldredge, J., Wang, C., 2009. High-amplitude pitch of a flat plate: an abstraction of perching and flapping. *International Journal Micro Air Vehicles* 1, 203–216.
- Platzer, M.F., Jones, K.D., Young, J., Lai, J.C.S., 2012. Flapping wing aerodynamics: progress and challenges. *AIAA Journal* 46, 2136–2149.
- Schnipper, T., Andersen, A., Bohr, T., 2009. Vortex wakes of a flapping foil. *Journal of Fluid Mechanics* 633, 411–423.
- Schouveiler, L., Hover, F.S., Triantafyllou, M.S., 2005. Performance of flapping foil propulsion. *Journal of Fluids Structures* 20, 949–959.
- Shyy, W., Lian, Y.S., Tang, T., Viieru, D.L., 2008. Aerodynamics of Low Reynolds Number Flyers. Cambridge University Press, New York.
- Wang, Z., 2005. Dissecting insect flight. *Annual Review of Fluid Mechanics* 37, 183–210.
- Webb, C., Dong, H., Ol, M., 2008. Effects of unequal pitch and plunge airfoil motion frequency on aerodynamic response. In: 46th AIAA Aerospace Sciences Meeting and Exhibition, Reno, NV. AIAA-2008-0582.
- Wu, J.C., 1981. Theory for aerodynamic force and moment in viscous flows. *AIAA Journal* 19, 432–441.
- Wu, J.C., 2005. Elements of Vorticity Aerodynamics. Tsinghua University Press, Beijing.
- Yu, M., Hu, H., Wang, Z., 2012a. Experimental and numerical investigations on the asymmetric wake vortex structures around an oscillating airfoil. In: 50th AIAA Aerospace Sciences Meeting, Nashville, TN. AIAA 2012-2299.
- Yu, M., Wang, Z., Hu, H., 2013. High fidelity numerical simulation of airfoil thickness and kinematics effects on flapping airfoil propulsion. *Journal of Fluids and Structures* 42, 166–186.
- Yu, M., Wang, Z., Hu, H., 2012b. Airfoil thickness effects on the thrust generation of plunging airfoils. *Journal of Aircraft* 49, 1434–1439.